This is a peer-reviewed, accepted author manuscript of the following article: Khodabux, W., Liao, C., & Brennan, F. (2021). Characterisation of pitting corrosion for inner section of offshore wind foundation using laser scanning. *Ocean Engineering*, *230*, [109079]. https://doi.org/10.1016/j.oceaneng.2021.109079

Characterisation of pitting corrosion for inner section of offshore wind foundation using laser scanning.

Waseem Khodabux [1, 2], Carole Liao[3] and Feargal Brennan[2]

1 Cranfield University, School of Water, Energy and the Environment, Renewable Energy Marine Structures - Centre for Doctoral Training (REMS-CDT), Bedfordshire MK43 0AL, United Kingdom; mohammud.khodabux@strath.ac.uk

2 University of Strathclyde, Department of Naval Architecture, Ocean & Marine Engineering, Glasgow G4 0LZ, United Kingdom; feargal.brennan@strath.ac.uk

3 Cranfield University, School of Aerospace, Transport and Manufacturing, Bedfordshire MK43 0AL, United Kingdom; c.liao@prismaticltd.co.uk

* **Correspondence:** mohammud.khodabux@strath.ac.uk, feargal.brennan@strath.ac.uk

Abstract

Pitting corrosion is a complex mechanism and has been found in the inner sections of offshore wind structures where the standards at the time indicated that those sections were water tight and therefore free from corrosion. Pits propagate and grow in size and this can have serious implications for the structural integrity of the structure by reducing the fatigue life but also under some conditions changing to a crack whereby the damage can be accelerated. In this study, pitting corrosion is extracted from coupons exposed to the unique inner environment of offshore structures for a duration of 528 to 1049 days and modelled with time by extracting their geometries, such as minor length, major length and depth using laser scans. A maximum pit depth of 1.67mm was observed. A series of analyses were run to understand the pitting mechanism and the effect of the stress concentration factor.

Keywords: Inner corrosion, laser scanning, offshore wind turbine, pit geometries, pit modelling

Introduction

Pitting corrosion is known to be the most dangerous form of marine corrosion. Various accidents in the marine world involving pitting corrosion have put it in the spotlight [1]. The necessity for this study stems from the underestimation of corrosion in the inner section of monopiles by designers in the early development of the offshore wind support structures that are currently in operation. The standards at the time dictated that corrosion protection was optional within the inner section of monopiles but due to

the failure of J-tube seals, open access hatches and other leakages, seawater has seeped into the inner compartments and created a unique environment for corrosion to thrive. The scale of the corrosion damage was only discovered upon inspection of the monopiles, with pitting corrosion identified as one of the forms of corrosion that were detected[2][3][4].

One of the methods used to gauge corrosion is the usage of corrosion coupons. A corrosion coupon is the simplest and most established method of estimating corrosion losses and further inspected to determine the corrosion mechanisms present. The corrosion coupon is made of the same material as the part/structure in operation and after a reasonable amount of time of exposure is weighed to determine the corrosion loss. The coupons are commonly prepared per ASTM G1 and G4 standards[5], [6]. In Figure 1, a coupon is shown before and after the cleaning. The holes are used as an attachment point to the structure.

Figure 1: Illustration of coupons[7]

In the case of offshore wind structures, a coupon made of steel of S355 grade similar to the structure is placed in the monopile and, upon exposure to the marine environment, corrodes reflecting the corrosion rate and the corrosion mechanism the structure is experiencing. The coupons used in this study have been exposed from between 528 to 1049 days and fully immersed inside a monopile. This gave a unique possibility to measure and count the various pits and model their evolution using a 3D laser scanner.

3D laser scanning is an effective tool and has a track record that is established in the engineering field. It has been used successfully in various applications, from

automotive to aerospace for inspection and also reverse engineering[8]–[10]. The spectrum of its application is wide and the resolution is continuously improving. Also, with better computing and processing power, this technology ensures smaller defects can be detected[11].

Despite corrosion being such a problem in the offshore wind industry, the literature is rather scarce on the characterisation of pitting corrosion in the inner section of monopiles.

The corrosion coupons were laser scanned and the data points collected were cleaned. Once done, the pits were extracted. The logic is expressed in Figure 2. An important aspect of this study is also to define a pit and assess the current practice in the industry. A fundamental distinction is made between general corrosion and pitting corrosion and is expressed quantitatively to distinguish both of them based on the pit depth.

From the laser scanning, the following dimensions were characterised:

- Pit detection and count
- Pit depth
- Pit major length and minor length
- Pit aspect ratio

A deterministic approach from the data allowed the different characteristics of the pits to be modelled and these are listed as follows:

- The number of pits to time
- The pit depth to time
- The pit major and minor lengths to time
- The pit aspect ratio to time
- The pit volume to time

Special attention has been given to the aspect ratio, and the minor and major lengths as those did not tend to be taken into consideration in the literature; the pit depth seemed to be the dominating factor and given more attention in the research community. For a structure such as an offshore wind turbine (OWT) where the bending loads are dominant, the stress concentrations as a result of the pits' dimensions were

dependent on the aspect ratio. Considering two pits with the same depth and having the same global stress, where Pit 1 is broad and Pit 2 is narrow, the latter would have a greater tendency to transform into a crack, thus accelerating failure of the component. In this study, those characteristics are documented to allow usage of those dimensions in a stress analysis context.

Due to the long exposure of the coupons, the pits are also assessed for the presence of the biological effects of corrosion, where the corrosion mechanism had been observed to shift from aerobic to anaerobic corrosion. Melcher's model is employed to do this and the average annual temperature of the North Sea is used as input as this model is temperature-dependent[12].

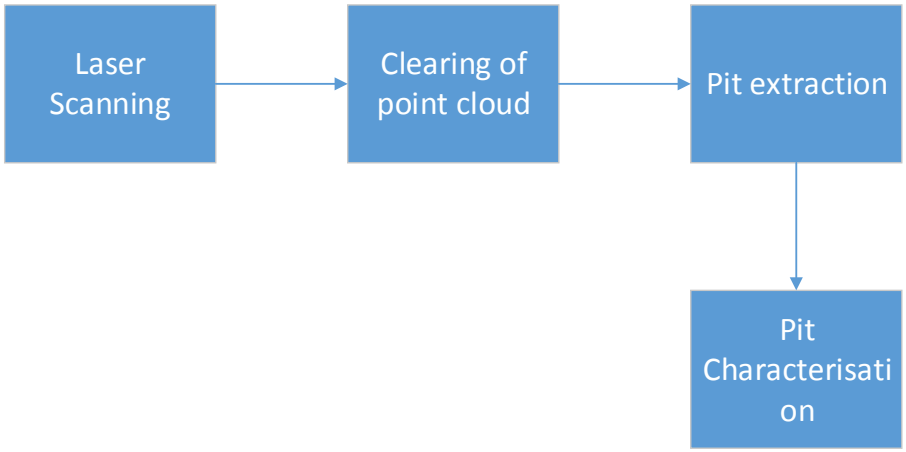

Figure 2: Flow process for coupon analysis

Methodology

To fulfil the goals set, the analysis will require the data acquisition of the corroded coupon topology using the laser scanner, the cleaning of the point cloud and finally the extraction and characterisation of the pit.

Laser Scanning

Laser scanning is a tool capturing 3D coordinates from a reference point. It requires the equipment and data acquisition software, which is usually installed on a portable computer. The main parameter is the resolution of the scan and this was set to 0.2mm. The particular scanner used could capture data points to a finer resolution, i.e. to 0.04mm; unfortunately, the acquisition system could not cope with this level of high resolution and, therefore, the second-best option had to be chosen, being 0.2mm.

Before the scans, the calibration plate was employed to correct any calibration errors with the machine.

The point cloud required some digital cleaning before effective usage shown in Figure 3.

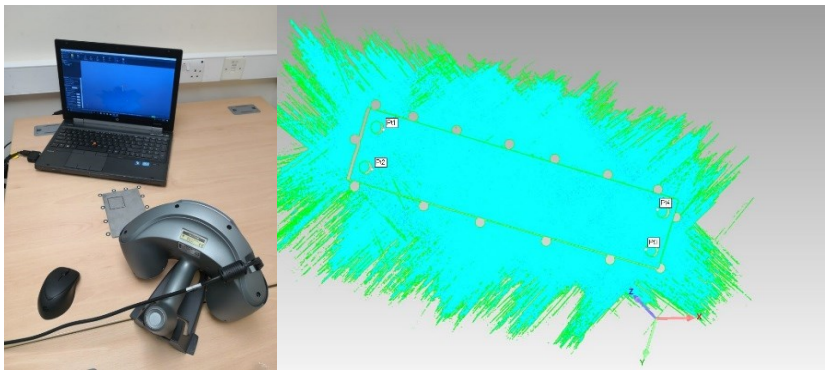

(a) **(b)**

Figure 3: (a)Laser scanning tool and (b) raw data cloud

Cleaning Cloud Point

Using Geomagic software, points surrounding the coupon were trimmed away and the data points were then exported shown in Figure 4.

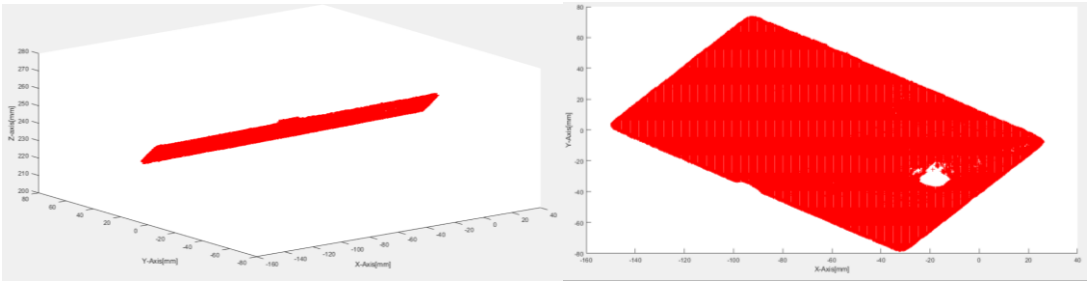

Figure 4: Cleaning of data points

Pits' Extraction and Characterisation

Pit Definition

The question as to what defines a pit is not related to the comprehension of a corrosion pit as a theoretical exercise. It is regarded instead in a more practical term and asks the following questions: What constitutes a pit? and What are the dimensions required for a pit to qualify as a pit? The latter is a more complex question than it sounds and tends to have more far-reaching consequences for inspection.

As a rule of thumb, pits and general corrosion are defined as such respectively[13]:

- Pitting corrosion, which refers to corrosion with length and width *less* than three times that of the uncorroded wall thickness
- General corrosion (wastage), which refers to corrosion with length and width *more* than three times that of the uncorroded wall thickness

This value should be viewed with a critical mindset and the following questions have to surface: Why three times, why not two or five in that regard? What is the impact of this definition of a pit on a thin-walled structure and thick-walled structure? Where does that value derive from? Another important point is that pits are very rarely characterised based on their length and width but instead on the depth. No studies have been done relating, for instance, to the extreme value of length and width of a pit. To shed light on that point, it is fundamental to think of a piece of steel of thickness 60mm, which is currently employed in offshore wind structures. If there is a corrosion defect that is 150mm in length and width but only a few microns in-depth, can that be defined as a pit? The problem compounds itself in the case where there is pit coalescence with one just smaller than 180mm and the other 50mm with a depth of 1mm and the other 5mm respectively, as an example. Is it general corrosion or is it pitting corrosion?

To address this problem, few conditions were employed to choose the pits as follows:

1. The areas registered smaller than 0.5mm^2 were neglected (smaller than that has proved to capture some noise. An example is shown in Figure 5 and the table illustrates the basis of the rejection.

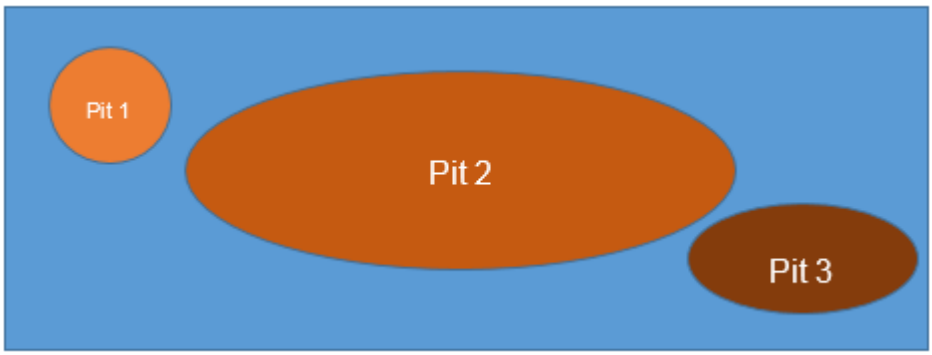

Figure 5: Area rejection

Table 1: Area of pits rejection table

Pit	Pit size [mm^2]	Algorithm output
Pit 1	0.2	Rejected
Pit 2	5.0	Accepted
Pit 3	0.5	Accepted

2. The depressions smaller than or equal to 0.2mm were neglected as they were considered to be general corrosion rather than pits and are shown in Figure 6 with Table 2 showing the rejection /acceptance table based on the example.

Figure 6: Pit depth

Table 2: Pit depth rejection

Defect name	Defect Depth[mm]	Algorithm output
Pit 1	0.15	Rejected
Pit 2	0.5	Accepted

3. The pits that were located 2mm from the edges were not taken into consideration due to edge effects shown in Figure 7 and Table 3 indicating the rejected defects.

Figure 7: Pit edge effects rejection

Table 3: Rejection table based on edge effects

Defect name	Distance from the edge[mm]	Algorithm output
Pit 1	0	Rejected
Pit 2	1	Rejected
Pit 3	2	Accepted
Pit 4	5	Accepted

For this study, the definition of a pit is taken as follows:

- The areas of the pits registered smaller than or equal to 0.5mm^2 were neglected (smaller pits have proved to capture some noise).
- The depressions of the pits smaller than or equal to 0.2mm are neglected as they were considered to be general corrosion rather than pits.
- The pits that were located 2mm from the edges were not taken into consideration due to edge effects.

The pits were characterised manually and, using the coordinates, the major and minor lengths were calculated using the distance formula.

Pit Major and Minor Length

The pit length was selected from a colour coded image once the pits were selected based on the three criteria established above. The two extremes were selected and using the distance formula the major length was calculated as shown in Figure 8.

$$\boldsymbol{Major\ length} = \sqrt[2]{(\boldsymbol{x_2} - \boldsymbol{x_1})^2 + (\boldsymbol{y_2} - \boldsymbol{y_1})^2} \qquad \textbf{Equation 1}$$

$$Minor\ length = \sqrt[2]{(x_3 - x_4)^2 + (y_3 - y_4)^2} \qquad \textbf{Equation 2}$$

Where (x_1, y_1), (x_2, y_2) are the major length coordinates that were chosen and (x_3, y_3), (x_4, y_4) are the minor length coordinates.

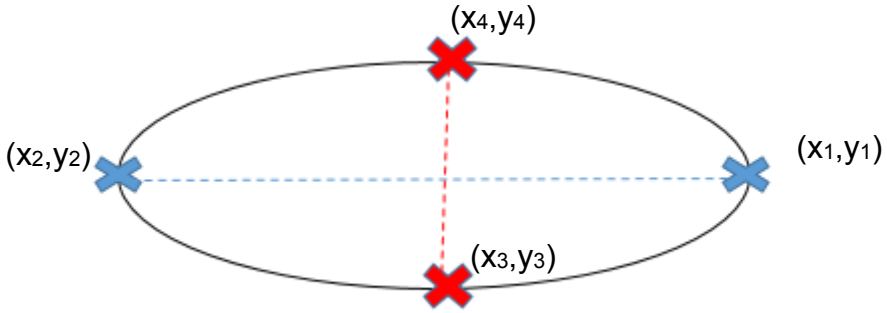

Figure 8: Coordinates selection for major and minor length

Pit projected area

Based on the major and minor lengths, the pits' projected area was calculated by approximating the pit geometry to an elliptical one. The formula for the area of the ellipse is

$$Area\ of\ Ellipse = \frac{\pi}{4}ab \qquad \textbf{Equation 3}$$

Where *a* is the major length and *b* is the minor length.

Pit depth and aspect ratio

To capture the actual pit's depth, a reference region must be defined for its measurement. This reference region is a function of the major and minor lengths' coordinates (extreme coordinates of pits) shown in red and blue from Figure 8. This region would be formed between two rectangles, the inner and outer one shown in Figure 9. The inner rectangle would have length and breadth equal to the major and minor lengths applied at the extreme coordinates and the outer rectangle will have the minor and major length increased by a factor of 1.2.

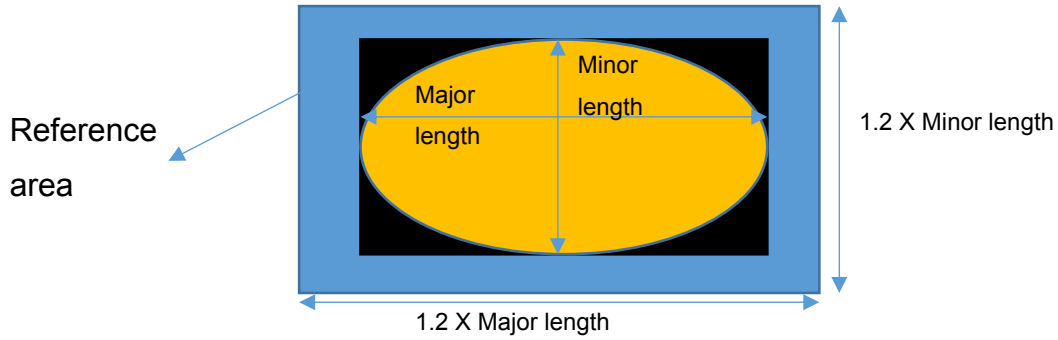

Figure 9: Reference area for pit measurements

The reference depth is computed by averaging all the depth coordinates in the reference area. The depth of the pit is calculated from subtracting the depth coordinates inside the pit to the reference depth. The reference regions are shown in Figure 10 with each pit surrounded by the turquoise coordinates as the inner rectangles and the red ones as the outer rectangles.

When referencing regions some of the points do lie outside the plate and in such a case only the existing data points inside the plates are considered.

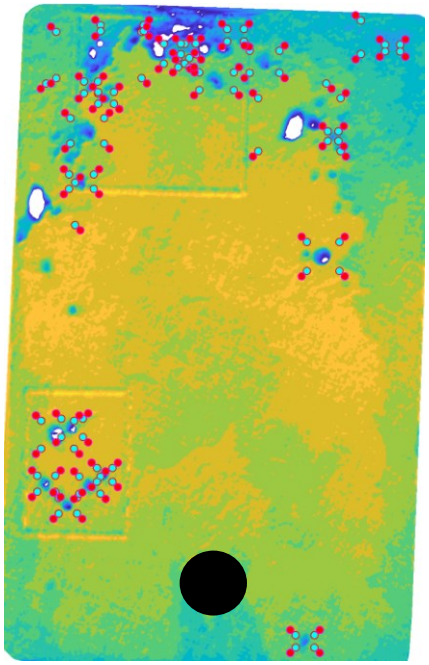

Figure 10: Pits' depth references

The aspect ratio of the pits is calculated as the ratio of the pit depth to the major length.

Pit depth is determined once the reference area is defined according to

$$Pit\ depth\ =\ average\ reference\ of\ pits - minimum\ point\ of\ pit$$ **Equation 4**

The aspect ratio is calculated as:

$$AR_{xz} = \frac{depth}{majorlength}$$ **Equation 5**

Pit models provided by the ASTM standards and various other papers show a tendency to be represented by the power curves. This fit will be investigated to calibrate the values of A and B to time for pit depth, major length, minor length and aspect ratio. The general equation is shown as:

$$Pit\ Characteristics = At^B$$ **Equation 6**

Where *A* and *B* are the constants to be calibrated, *t* is the time.

Results

The cleaned data are shown below as a contour image.

It has to be stated that the Figure 11 shown has a tilt due to a gyroscopic error in the orientation of the laser scanner which could not be resolved with the calibration block provided by the manufacturer. There have been attempts made to rotate the point cloud but it was observed that the data required for the collection were unaffected by correcting the tilt. Also for the coupons of those dimensions, more than three million data points were collected. Any significant manipulation is time-consuming and requires a significant amount of both computational effort to be effectively performed.

From Figure 11, the regions denoted by the dark blue are the ones used as pits. The black circle is an omitted region due to the attachment hole for the coupon.

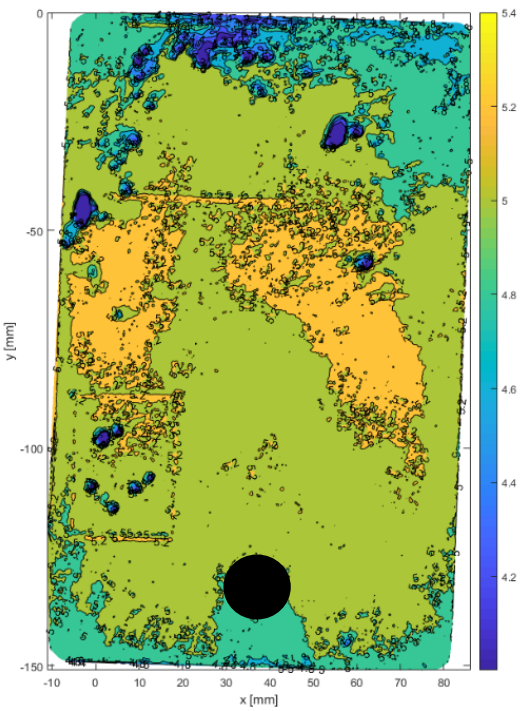

Figure 11: Coupons with pits indicated by the blue region

The number of pits for each coupon is tabulated is shown in Table 4.

Table 4: Number of pits

Coupon Number	Number of days exposed	Number of Pits
285	528	14
234	528	18
187	538	8
385	560	9
169	590	27
329	590	29
47	600	28
1424	802	30
8	1049	12

For each of the coupons, the pit characteristics were extracted, and the results are displayed in Figure 12. The plots take into account, the minimum, maximum and average/mean for each of the pits' characteristics to provide an envelope for the variation of the pits.

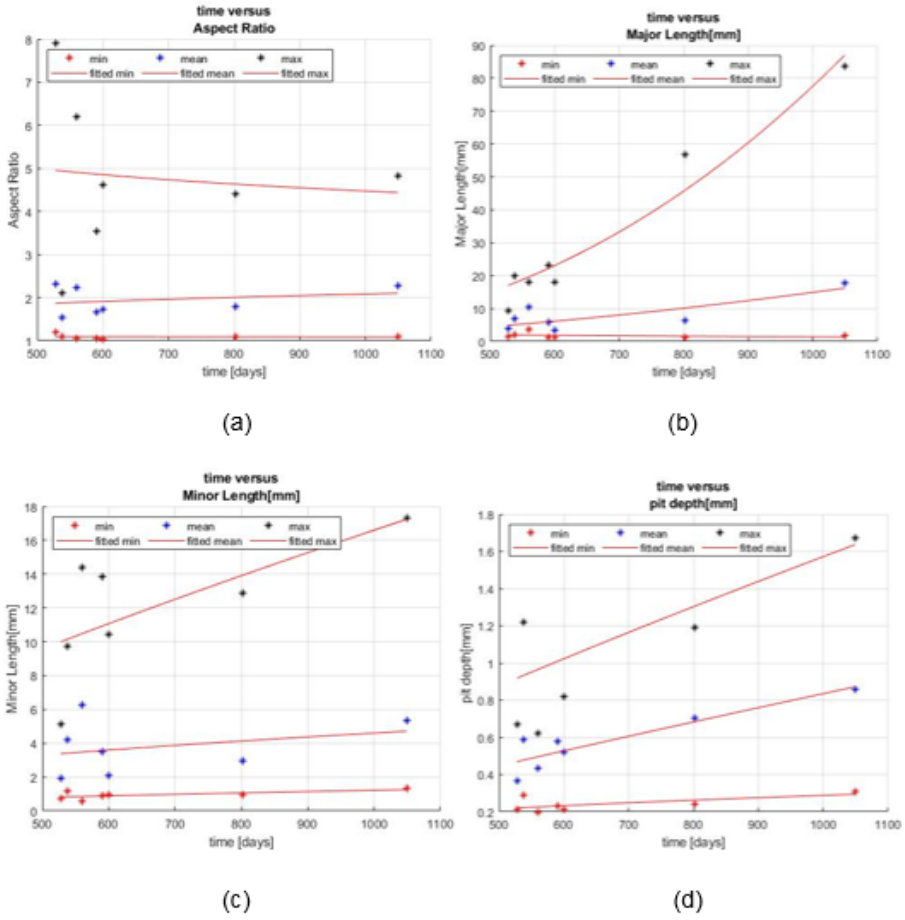

Figure 12: Characteristics envelope plotted with time where (a) is the time vs aspect ratio, (b) is the major length vs time, (c) is the minor length vs time and (d) is the time vs depth.

Discussion

Filters

The filters used for pit characterisation have to be carefully included. Figure 13 shows the effects of using those to the definition of a pit. Initially, the red dots represent all the pits that would be found with only the filter of the pit depth. By applying the filter of the pit position, the blue and green pits only are chosen. Finally by applying the filter of the area the green pits are obtained which represent a more realistic observation of the pits on the coupon.

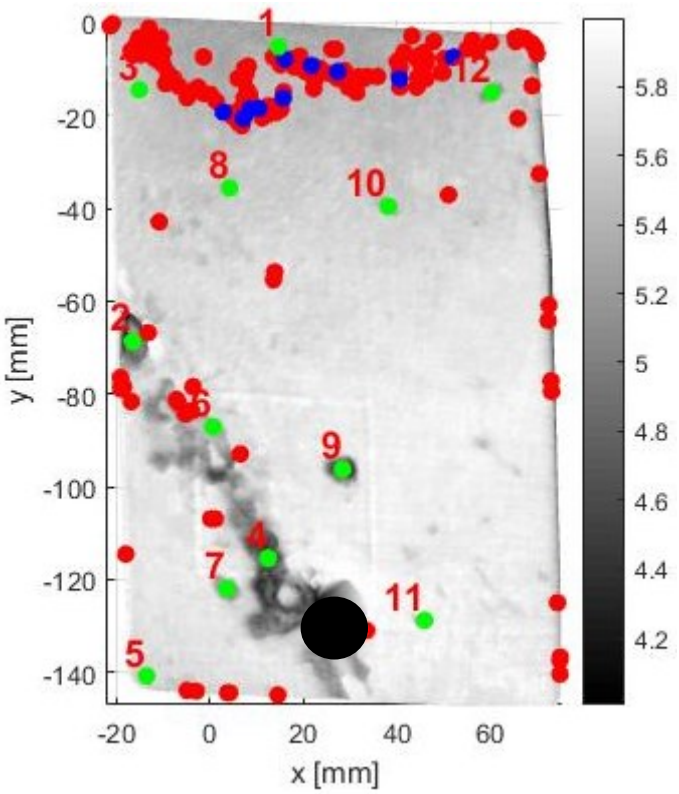

Figure 13: Pit filters

The choice of those filters was calibrated based on the best representation of the pits and the extraction process. The black dot indicates a region that had not been accounted for in the analysis as it represented the coupon attachment hole. Nota Bene: The number 4 pit denoted in the diagram is the longest pit registered in the analysis of the coupon. By traditional definition, this pit would be counted as general corrosion. It had all the characteristics of localised corrosion and therefore in this study is taken to be a pit.

Aerobic vs. anaerobic corrosion models

The plots fitted with power curves (Figure 12) have the following values (Table 5) for the constants. It has to be mentioned that those values provide an envelope for the pitting corrosion model for the duration of the number of days. Corrosion is such a complex process that further investigation will have to occur for shorter exposure of the coupons.

Table 5 shows the values of A and B for the pits' characteristics.

Table 5: Power-law constants for data fit

	Minimum		Mean		Maximum	
	A	B	A	B	A	B
Area[mm^2]	0.433	0.179	1.000	3.684	1.000	3.127
Major Length [mm]	56.728	0.000	1.000	1.734	1.000	2.374
Minor Length [mm]	0.017	0.618	0.164	0.483	0.069	0.794
Aspect Ratio	1.154	0.000	0.648	0.169	13.478	0.000
Pit Depth [mm]	0.016	0.417	0.002	0.900	0.005	0.841

In this model, however, it must be investigated if the power curves represent the aerobic model or the anaerobic one. To do so, it is important to distinguish the pits that are under the aerobic and the anaerobic influence and finally try to combine both of them to represent a full combination of the models for the classification of the values of A and B. The average temperature of the North Sea has been taken to be 10.5ºC and the threshold to represent the transition from aerobic to anaerobic corrosion was determined using Melcher's model[14].

Melcher's model-Figure 14 is built up of 4 different sections representing various corrosion mechanisms and taking into account both the environment and also the diffusion effects due to the rust layer at the surface that substantially reduces the corrosion rate[12]. The marine growth and the respiration mechanism involved due to this colonisation changes nature from an aerobic form to an anaerobic one when enough layers have grown[14]. This constitutes a different form of mechanism that needs to be reflected in the model. The importance of this section is vital as it does have a considerable effect on the pit depth and its growth rate. When the pit is totally soaked in this anaerobic environment, it then finally evolves into a linear form. Table 6 summarises all the steps in the Melcher's model.

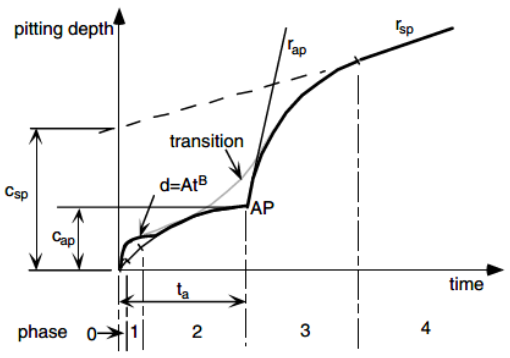

Figure 14: Melcher's model

Table 6: Description of Melcher's model [14]

Phase	Phase description and corrosion controlling mechanism
0	Initial pit growth
1 and 2	Pit growth under overall aerobic conditions under rust cover
3	Rapid pit growth under overall anaerobic conditions under rust cover
4	Steady pit growth under overall anaerobic conditions under rust cover

$t_{a:}$ exposure time under aerobic conditions.

c_{ap}: depth of pit under aerobic conditions

r_{ap}: corrosion rate of pit under aerobic conditions

c_{sp}: depth of pit under anaerobic conditions

r_{sp}: corrosion rate of pit under anaerobic conditions

All the above terms are dependent on annual mean temperature (T)

AP: transition from aerobic corrosion to anaerobic corrosion

The transitions can be calculated as a function of the average yearly temperature.

The maximum pit depth and minimum pit depth for the trend were used to investigate if a transition might have happened and, if so when it happened.

Finding the transition depth from aerobic to anaerobic for a temperature of 10.5ºC yields a depth of 0.5735mm. Comparing the minimum and maximum pit depth from the envelope yields an interesting result in that all the resulting maximum pit values are considered to be under anaerobic corrosion and all the minimum are aerobic ones. This implies two things: either simultaneously there is aerobic and anaerobic corrosion happening and that this is site dependent on the coupon, or that new pits formed due to general corrosion removing the surface and eating the pits up and as a result, the birth of those new pits are in an anaerobic form. Those have to be thoroughly

investigated in a controlled environment for more informed reasoning. Mathematically modelling pitting corrosion from the birth of the pits by using the data, required a combination of the aerobic and anaerobic models. The use of the mean depth is thus preferred.

It must be stated that there is a mix of mechanisms but in this model, it is going to be assumed that once the mechanism is anaerobic it would not revert.

Following the above logic, the pit depth to time is shown in Figure 15 for both the aerobic and anaerobic corrosion. To reduce the effects of duplication (same number of days the coupon is exposed to corrosion), the average of the mean pit depth has been found. The orange section shows the aerobic corrosion and the grey one the anaerobic.

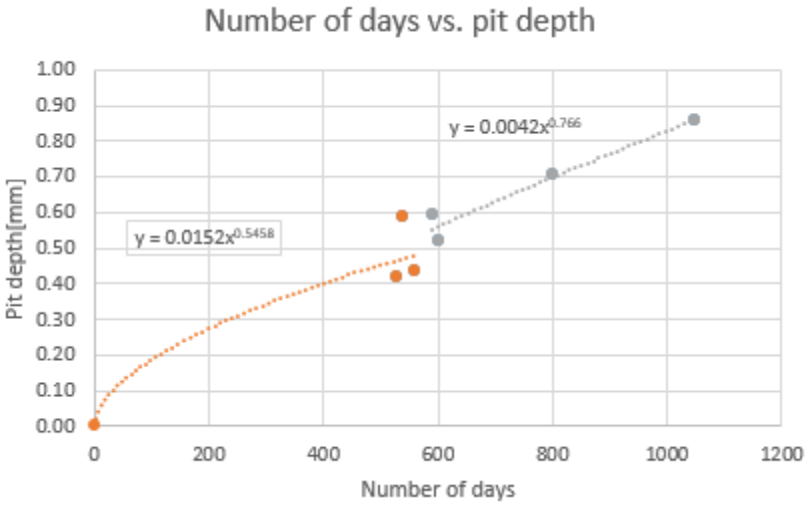

Figure 15: Aerobic and anaerobic mechanisms

Using those values, when compared with Melcher's model, a clue to the mechanism of corrosion can be investigated. As an example of the maximum pit depth and using the average temperature of the North Sea of 10.5ºC, the transition to a biological one takes approximately 570 days.

Effects of pit coalescence

The number of pits, when plotted against time, shows a pattern that seems to promote the idea of pit coalescence. As the number of pits grows in length and width, they merge. This can be beneficial in terms of the SCF as when they coalesce the pits' aspect ratio decreases with time. This pattern seems to be cyclical, i.e. the number of

pits increases and then decreases; this is due to general corrosion chasing the pitting corrosion until the former consumes the pit. This can be considered as a new layer being removed and another one being formed, and new pits being created. This mechanism must be observed more regularly and for a longer duration.

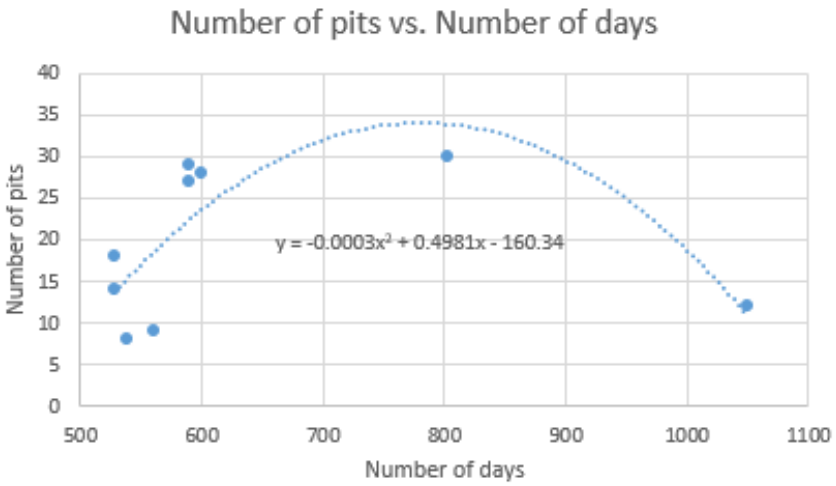

Figure 16: Number of pits vs. days

The number of pits can seem rather difficult to comprehend due to a cyclical form of corrosion demonstrated in Figure 16. It can be viewed in a different form considering total volumetric loss due to pitting corrosion to time. The pits were all assumed to be semi ellipsoidal and their respective volume was calculated using the following equation:

$$V = \frac{2}{3}\pi abc$$ **Equation 7**

Where *a* is the half major length, *b* is the half minor length and *c* is the depth.

Despite the number of pits decreasing from year 1 to 3, the volume loss increases to time. The pits are thus coalescing and growing in size as shown in Figure 17 following a quadratic fit.

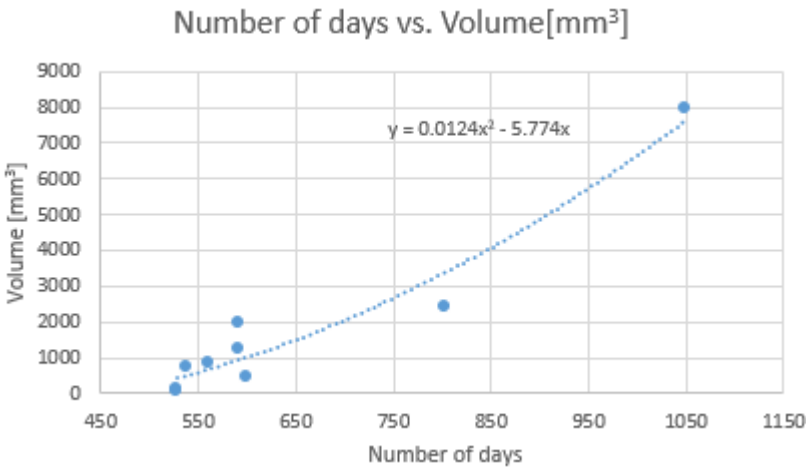

Figure 17: Volume of pits vs. time

Coupon comparison front and back

The coupon has been scanned both in the front and the back for this study shown in Figure 18. The reason is to show the difference in the corrosion of both the sides and relate it to the common practice of painting one side of the coupons and leaving the other exposed shows the front and back surfaces of corrosion coupon 47. It can be seen that the front surface has been more attacked by general corrosion than the back one.

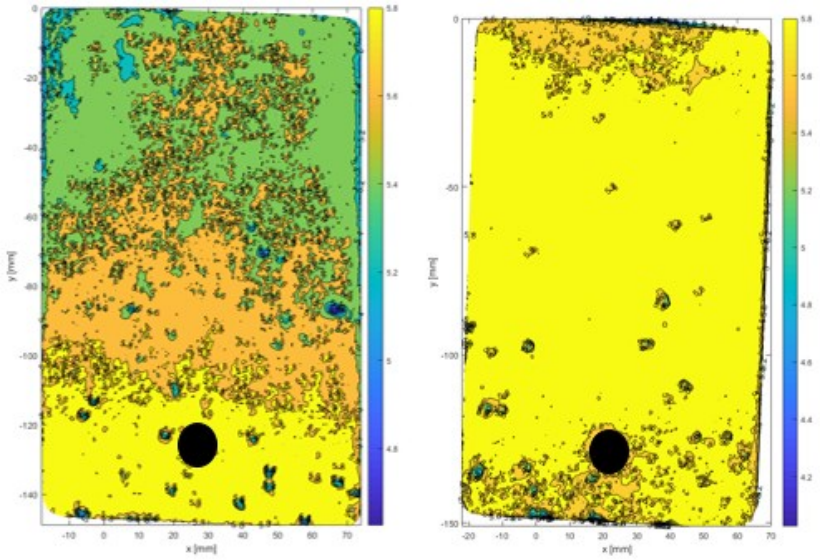

(a) (b)

Figure 18: Same coupon side comparison, (a) showing the front and (b) the back.

The regions of green and orange on the front sideshow layers of general corrosion that makes the surface corrosion loss more important than on the yellow regions on the backside. The orientation of the plates does have a substantial effect on the coupons. Unfortunately, no details were taken of the orientation when the coupons were picked up, i.e. if the more corroded surface was facing up or down in the environment. Based on the difference observed it would be highly advisable to monitor the orientation of the plate in such a confined environment.

A second interesting observation in the front plot (Figure 18) was the reduction of pits in the green region where the general corrosion was more prominent than on any other part of the coupon. This observation tallied with the fact that the higher level of general corrosion considerably reduced the pitting/localised corrosion impacts.

The difference in the pitting characteristics were tabulated in terms of their means as shown in Table 7.

Table 7: Difference in coupons

	Coupon Front	Coupon Back	The difference in localised corrosion[%]
Number of pits	28	19	32.14
Pit Major Length[mm]	3.52	3.23	10.51
Pit Minor Length[mm]	2.08	1.97	12.01
Pit Depth[mm]	0.51	0.46	13.72

SCF evolution of pits

The stress concentration factor for semi-elliptical pits is given by equation as follows[15].

$$K_t = \frac{1 + 6.6(\frac{a}{2c})}{1 + 2.2(\frac{a}{2c})}$$ **Equation 8**

Where K_t is the SCF; a the depth and c is half the minor length.

It has to be noted that the aspect ratio decreases and as a result, the SCF will follow the same path as the pit is becoming 'blunter' with time due to the major length increasing at a faster rate than the pit depth. The above equation does not take in consideration the change in thickness of the material and only the geometry of the pit.

The variation in the aspect ratio of the pits provides the stress that will be experienced by the structure under uniaxial tension shown in Figure 19.

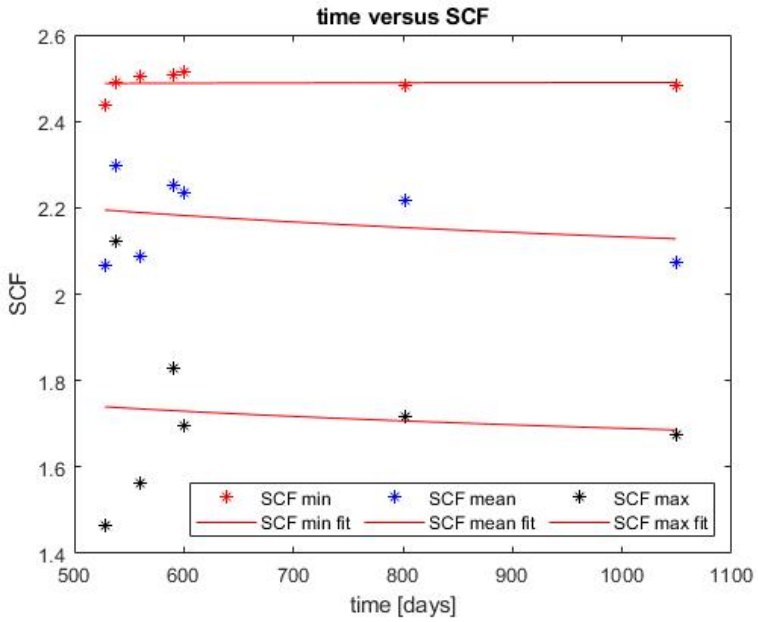

Figure 19: SCF vs. time

The stress concentration factor decreased considerably over time. **The SCF though needed to come with a warning as it did not give a complete picture of the stress at the pit.** The local stress had to be calculated and the SCF must not be used as a measure of damage. It is the local stress that results from the combination of the loss of thickness and the pitting corrosion that has to be used.

Conclusions

- A new definition of pits in a quantitative manner and its implementation to laser scanning.

- Over time, the number of pits decreases and this is explained as the effect of pit coalescence increases with time as demonstrated by the quadratic growth of the volume of the pits with time.
- The corrosion pit power model growth commonly used has been calibrated for the pit area, major length, minor length, aspect ratio and depth in an envelope from the minimum, mean and maximum.
- A maximum pit major length of 83.6 mm, minor length 17.3mm and a pit depth of 1.67mm.
- Some of the pits were also observed to be under the influence of anaerobic/biological corrosion when tested against Melcher's model and a pit depth model was developed showing this effect which shows a transition happening from aerobic to anaerobic after 570 days.
- A superficial consideration of the SCF of larger pits had been done but it is local stress that is important and it is recommended that further work be carried out to determine the stress state.

Acknowledgments: This work was supported by grant EP/L016303/1 for Cranfield University, the University of Oxford and Strathclyde University, Centre for Doctoral Training in Renewable Energy Marine Structures (REMS) (http://www.rems-cdt.ac.uk/) from the UK Engineering and Physical Sciences Research Council (EPSRC).

Conflicts of Interest: "The authors declare no conflict of interest."

Data Availability: The raw/processed data required to reproduce these findings cannot be shared at this time as the data also forms part of an ongoing study.

REFERENCES

[1] J. Bhandari, F. Khan, R. Abbassi, V. Garaniya, and R. Ojeda, “Modelling of pitting corrosion in marine and offshore steel structures - A technical review,” *J. Loss Prev. Process Ind.*, vol. 37, pp. 39–62, 2015, doi: 10.1016/j.jlp.2015.06.008.

[2] A. R. Black and P. K. Nielsen, “Corrosion protection of offshore wind farm structures – present understanding and future challenges,” 2011, no. September, pp. 1–9.

[3] L. R. Hilbert, T. Mathiesen, A. R. Black, C. Christensen, and F. Technology, “Mud zone corrosion in offshore renewable energy structures,” *Eurocorr 2013*, no. Mic, pp. 1–5, 2013.

[4] B. A. R. Black , P. K. Nielsen, FORCE Technology, “Corrosion protection of offshore wind farm structures – present understanding and future challenges,” *Eurocorr 2011*, no. September, pp. 1–9, 2011.

[5] ASTM, “ASTM G1:Standard Practice for Preparing, Cleaning, and Evaluating Corrosion Test Specimens,” 1999.

[6] Astm, “ASTM G4 Standard Guide for Conducting Corrosion Coupon Tests in Field Applications,” *ASTM Stand.*, 2004.

[7] W. Khodabux, P. Causon, and F. Brennan, “Profiling Corrosion Rates for Offshore Wind Turbines with Depth in the North Sea,” pp. 3–7, 2020, doi: 10.3390/en13102518.

[8] S. Son, H. Park, and K. H. Lee, “inspection,” vol. 42, pp. 889–897, 2002.

[9] K. H. Lee and H. Park, “Automated inspection planning of free-form shape parts by laser scanning,” vol. 16, pp. 201–210, 2000.

[10] C. Zhang and D. Arditi, “Automation in Construction Automated progress control using laser scanning technology,” *Autom. Constr.*, vol. 36, pp. 108–116, 2013, doi: 10.1016/j.autcon.2013.08.012.

[11] T. Tóth and J. Živčák, “A Comparison of the Outputs of 3D Scanners,” *Procedia Eng.*, vol. 69, pp. 393–401, 2014, doi: 10.1016/j.proeng.2014.03.004.

[12] R. E. Melchers, “Modeling and prediction of long-term corrosion of steel in marine environments,” *Int. J. Offshore Polar Eng.*, vol. 22, no. 4, pp. 257–263, 2012.

[13] A. Cosham, P. Hopkins, and K. A. Macdonald, “Best practice for the assessment of defects in pipelines - Corrosion,” *Eng. Fail. Anal.*, vol. 14, no. 7, pp. 1245–1265, 2007, doi: 10.1016/j.engfailanal.2006.11.035.

[14] R. E. Melchers, “The effect of corrosion on the structural reliability of steel offshore structures,” *Corros. Sci.*, vol. 47, no. 10, pp. 2391–2410, 2005, doi: 10.1016/j.corsci.2005.04.004.

[15] M. Cerit, K. Genel, and S. Eksi, “Numerical investigation on stress concentration of corrosion pit,” *Eng. Fail. Anal.*, vol. 16, no. 7, pp. 2467–2472, 2009, doi: 10.1016/j.engfailanal.2009.04.004.